RESEARCH ARTICLE

The effect of slope and number of arms on the structural properties of square tower-like manganese thin films

M. Fakharpour

Department of Material Engineering, Maybod Branch, Islamic Azad University, Maybod, Iran

ARTICLE INFO

Article History:
Received 2020-05-10
Accepted 2020-07-16
Published 2021-02-01

Keywords:
Square tower-like thin films
Manganese
Slope
Arms

ABSTRACT

In this work, square tower-like manganese (STMn) thin films on glass substrates using were obtained using Glancing Angle Deposition "GLAD" technique. Three types of nanostructures are prepared with different number of arms and different slopes by placing a shadowing block in the center of the substrate holder. The structural characterization of the obtained thin films was investigated using field emission scanning electron microscope (FESEM) and atomic force microscope (AFM). Results showed that the slope angle (α), the grain size, porosity and surface roughness of the films decreases with increasing distance from the edge of the shadowing block (decreasing the slope of nanostructure). Structural properties of thin films were obtained using X-ray diffraction (XRD). The intensity of the main peak of STMn with 8 arms and 10 arms increases and STMn with 9 arms decreases with increasing the edge of the shadowing block. The results show that the strain on the nanostructures of the STMn with 8 arms and STMn with 10 arms decreases with increasing distance from the edge of the shadowing block due to the increase in the intensity of the main peak. While strain on the nanostructure of the STMn with 9 arms increases with increasing distance from the edge of the shadowing block.

How to cite this article
*Fakharpour M. The effect of slope and number of arms on the structural properties of square tower-like manganese thin films. J. Nanoanalysis., 2021; 8(1): -10. DOI: 10.22034/jna.***.*

INTRODUCTION

Glancing angle deposition (GLAD) technique is a type of physical vapor deposition (PVD) process that has interested many researchers today. This technique with a vapor incident angle greater than 85° is an oblique angle deposition technique (OAD) process with a vapor incident angle less than 85° with rotation of the substrate holder in different directions [1,2]. Three dimensions nanostructures with different morphologies such as vertical columns [3], helical [4], and zigzag shapes [5], and star-like [6] can be fabricated with GLAD technique. In addition, these films are used in solar cells [7], optical filters [8], and gas sensors [9] due to their controllable porosity.

Manganese is widely used in nature due to its low cost, high abundant and environmentally friendly nature. This metal is usually found in the form of oxides with four different crystalline phases such as MnO, MnO_2, Mn_2O_3, and Mn_3O_4 that have different structural and compositional properties. Thin films of these oxides can be used in energy storage devices [10], supercapacitors [11], and the production of soft magnetic materials [12]. Manganese oxide thin films had been fabricated by various techniques such as RF magnetron sputtering [13], pulsed laser deposition [14], atomic layer deposition [15], sol-gel technique [16], and etc. GLAD technique due to its flexibility in changing deposition parameters such as temperature, gas pressure, and changing device parameters such as deposition angle, target distance from the substrate, rotation of substrate holder and also reproducibility is the best technique to fabricate thin films with pre-designed morphology. Brett and Krause [17] by using the OAD technique in conjunction with rotation of the substrate holder about its surface normal while

* Corresponding Author Email: *Mahsa.fakharpour@yahoo.com*

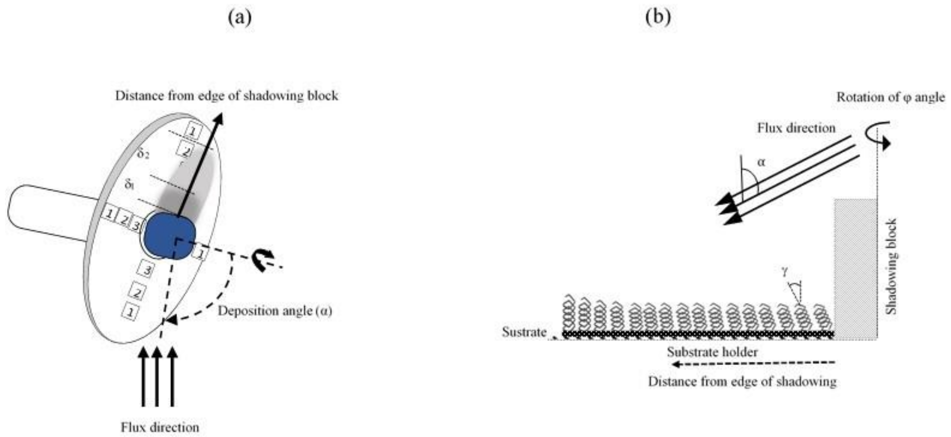

Fig.1. (a) Schematic of GLAD deposition and a shadowing block fixed at the center of the substrate holder; (b) Production of square tower-like Mn nanostructures.

they had fixed a shadowing block at the center of the substrate holder produced helical nano-structures called graded chiral nano-sculptured thin films. Savaloni el al. [18] fabricated chiral zig-zag silver thin films by placing a shadowing block in the center of the substrate holder using the GLAD technique. As the distance from the shadowing block increases, the slope of these nanostructures (angle of the chiral axis with the substrate surface normal (g)) decreases. Therefore, the nanostructured properties and grain size vary according to the distance from the shadowing block. In the present work, manganese thin films were fabricated using a deposition angle of 85° as square tower-like nanostructures tilted toward the incident deposition direction where a= 85° is the deposition angle between the incident flux direction and the substrate surface normal. Square tower-like thin films were produced by GLAD method with the substrate rotation sequentially at 90°. In addition, the length of the square side of each pitch decreases with increasing layer thickness. The structural and morphological properties of these nanostructures are studied as a function of distance from the edge of the shadowing block and the number of arms. Also, the crystallinity degree, grain size and strain of the square tower-like Mn thin films are studied as a function of the slope of nanostructure and the number of arms.

EXPERIMENTAL DETAILS

The all glass substrates were ultrasonically cleaned in acetone then ethanol before being introduced into the vacuum system. The substrate holder was selected a stainless steel disc with a diameter of 12 cm. At the center of this disc a cylindrical block (2 cm in diameter and 2.0 cm in height) was fixed as a shadowing block. The substrates were fixed at 1, 3 and 5 cm distance from this shadowing block along four mutually normal radii of the substrate holder disc. The square tower-like manganese (STMn) thin films were deposited on glass substrates of rectangular shape (2 1.8 cm^2) by electron beam evaporation using the GLAD technique (Edwards E19 A3 coating plant) at room temperature. The substrates were placed above the source at a distance of 30 cm. The base pressure was before the deposition 2×10^{-7} mbar. The deposition angle a is the angle between the incident flux direction and the substrate normal which was fixed at 85°. To produce each square tower-like nanostructure arm, the substrate holder was rotated clockwise with azimuthal angle φ =90 °. Hence, in each run four sets of three samples were produced for use in different analyses and reproducibility check of the samples. Three different square tower-like nano-sculptured thin films containing different number of arms, namely eight, nine and ten arms were produced. Each arm of the first pitch was deposited for 110 nm while each arm of the second and third pitches was 72 nm and 36 nm, respectively. Figs. 1(a and b) show the schematic drawing of the deposition system and growth behaviour of square tower-like nanostructures. The deposition rate was fixed at 1.0 Ås$^{-1.}$ Film thickness and deposition rate were measured using a quartz crystal deposition rate controller (Sigma Instruments, SQM-160, USA) positioned close to and at almost the same azimuthal angle as that of the substrate. The square tower-like nanostructures were characterized

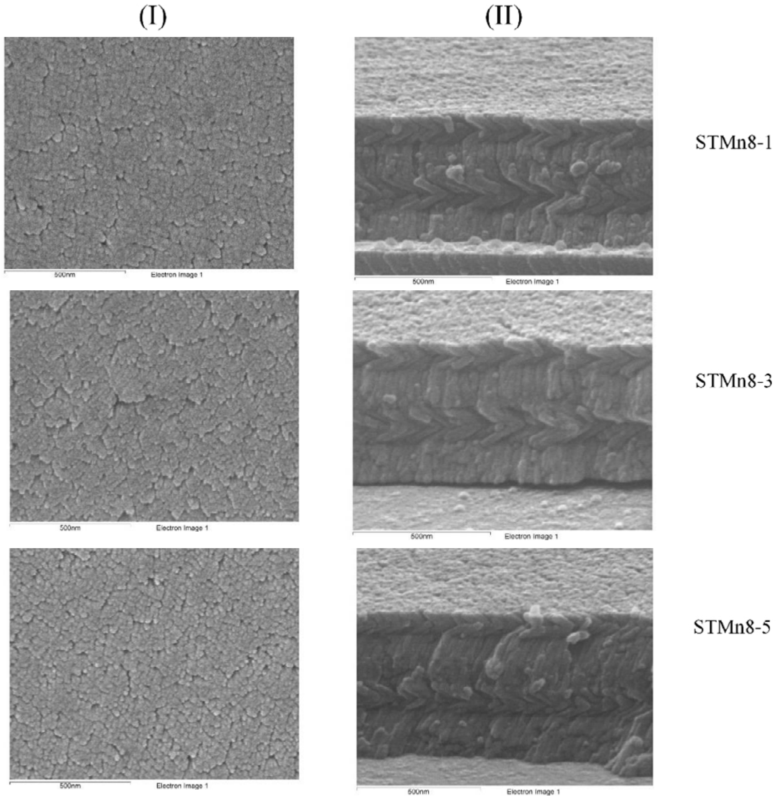

Fig. 2. FESEM images of the surface (column (I)) and cross section (column (II)) of the square tower-like Mn nanostructures with eight arms at three different distances of 1, 3 and 5 cm from the edge of the shadowing block.

by field emission electron microscope (FESEM) (Hitachi S-4100 SEM, Japan). The crystalline phase and crystal orientation of these films were examined using a Siemens D500 x-ray Diffractometer (CuK_α radiation; λ = 0.154056 nm and 40 kV, 30 mA) with a step size of 0.02° and count time of 1 sec/step. The surface physical morphology and roughness was obtained by AFM (NT-MDT, SOLVER, Nova Tech) analysis with a Si tip of 10 nm in diameter and in non-contact mode.

RESULTS AND DISCUSSIONS

The samples prepared in three stages of the experiment with the different number of arms (8, 9, and 10 arms) that each step contains of three different samples which were placed at different distances of 1, 3, and 5 cm from the edge of the shadowing block, we have encoded them as follows; The square tower-like manganese nanostructures with 8 arms are named as STMn8-1, STMn8-3, and STMn8-5 at different distances of 1, 3, and 5 cm from the edge of shadowing block. Similarly, for the nanostructures 9 arms we named them STMn9-1, STMn9-3, and STMn9-1 and for nanostructures with 10 arms we assigned them as STMn10-5, STMn10-3, and STMn10-1. The first number indicates the arms number of STMn nanostructure and the second number indicates the sample distance from the shadowing block in centimeter.

Structure and surface morphology of the square tower-like manganese thin films (STMn)

Fig. 2 (columns I and II) shows the FESEM images of the surface and a cross section of the STMn thin films with eight arms fabricated at three different distances of 1, 3 and 5 cm from the edge of the shadowing block. The structure of the grown nano-columns and the dense underlayer of the films [19, 20] are clearly recognizable in these images. The grown arms of the square chiral nanostructure and their angles, as well as the slope angle of the columns are observed. In addition, the length of the arms has been reduced from the lower square of the upper squares of the tower, which, according to the deposition experiment, the length of the arms is 110 nm, 72 nm and 36

Table 1. Estimated values of structural parameters for the square tower-like Mn thin films.

	STMn10					STMn9					STMn8				
X (cm)	γ(°)	H (nm)	P (%)	R_{rms} (nm)	R_{ave} (nm)	γ(°)	H (nm)	P (%)	R_{rms} (nm)	R_{ave} (nm)	γ(°)	H (nm)	P (%)	R_{rms} (nm)	R_{ave} (nm)
1	14	465.45	13.32	2.24	1.75	12	436.74	19.04	2.87	2.23	12	417.39	22.92	3.42	2.60
3	8	504.09	13.19	1.68	1.33	8	450	16.44	2.86	2.20	5	441	29.32	3.28	2.57
5	4	550.84	9.60	1.5	1.20	4	544.8	12.87	2.58	1.96	3	525	19.55	2.6	2.03

X is distance from the edge of the shadowing block; γ is slope angle; H is thickness of the film; P is surface void fraction (porosity); R_{ave}, R_{rms} and are average and root square surface roughness

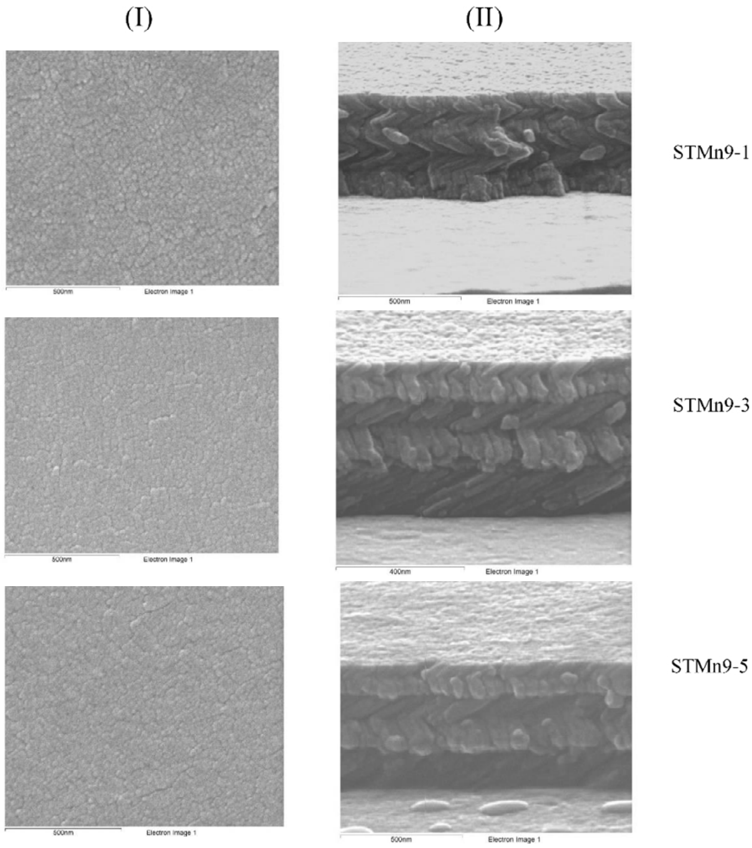

Fig. 3. FESEM images of the surface (column (I)) and cross section (column (II)) of the square tower-like Mn nanostructures with nine arms at three different distances of 1, 3 and 5 cm from the edge of the shadowing block.

nm, respectively, for different squares of the tower. The slope angle and the thickness of the STMn thin films with different number of arms are measured from the FESEM images and are given in Table 1. The shadowing block is the cause of change in the growth and the slope of the nanostructures of STMn. In FESEM images, it can be seen that as the distance from the edge of the shadowing block increases, the slope angle (g) decreases and the diameter of the square arms of the nanostructure increases. Further details of the effect of shadowing on the deposition are given in reference [18, 21]. The FESEM images of the surface of the STMn thin film with eight arms also show that the grain size and porosity of the film decreases with increasing distance from the edge of the shadowing block.

Figs. 3 and 4 (columns I and II) show the FESEM images of the surface and cross section of the STMn thin films with nine and ten arms fabricated at three different distances of 1, 3 and 5 cm from the edge

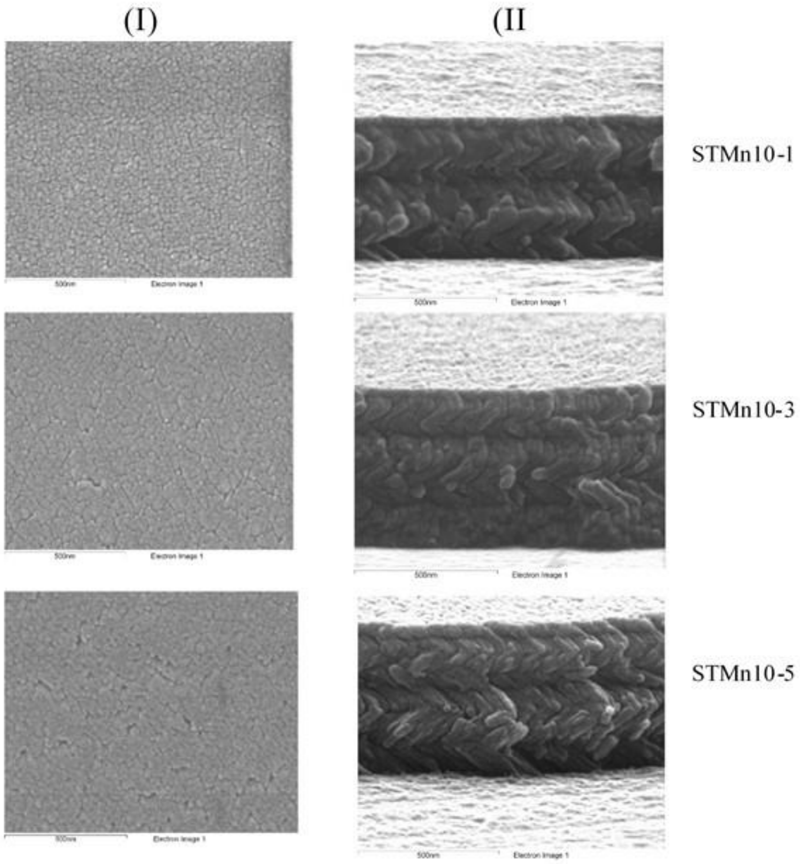

Fig. 4. FESEM images of the surface (column (I)) and cross section (column (II)) of the square tower-like Mn nanostructures with ten arms at three different distances of 1, 3 and 5 cm from the edge of the shadowing block.

of the shadowing block. All STMn samples with 9 and 10 arms are similar to the STMn nanostructure with 8 arms showing a square tower-like structure, but the slope of the nanostructures, the porosity, and the grain size are different. By measuring the slope of nanostructures of STMn thin film from cross section images, it is concluded that the slope of nanostructures, the grain size and porosity of the film decreases with increasing distance from the edge of the shadowing block, which corresponds to the results of STMn8 samples.

The effect of slope of STMn nanostructure on the morphology, grain size distribution and surface roughness were studied using AFM images of samples STMn with eight, nine and ten arms fabricated at three different distances of 1, 3 and 5 cm from the edge of the shadowing block. Figs. 5-7 represent two-dimensional and three-dimensional AFM images (columns I and II) along with surface volumetric fraction/porosity (column III) of material of the samples. The quantities of porosity, average and root mean square surface roughness (R_{ave}, R_{rms}) that measured using JMicro Vision software for STMn thin films are given in Table 1. Results in Table 1 for each group of samples (i.e., STMn8-1 to -5, STMn9-1 to -5 and STMn10-1 to -5) indicate that the porosity and the surface roughness of the samples are reduced by increasing the distance from the edge of the shadowing block. In other words, the samples become denser with a lower slope. It is observed by comparing the surface images in Figs. 2-4, that the surface smoothness is increased by decreasing the distance from the edge of the shadowing block. Comparing the surface roughness and the porosity of all three STMn samples with 8, 9 and 10 arms in Table 1, it is concluded that the surface roughness and porosity decrease with increasing number of arms. Because smaller and wider arms are formed on the surface of the layer by increasing the number of arms.

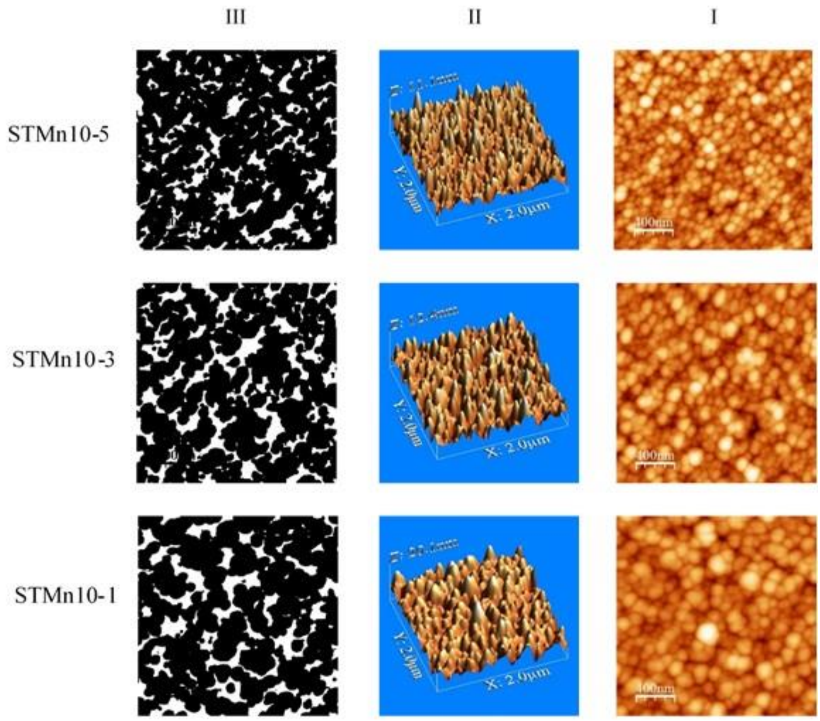

Fig. 5. AFM images of square tower-like Mn nanostructures produced at different distances of 1, 3 and 5 cm from the edge of the shadowing block with 10 arms; column (I) 2D images, column (II) 3D images, column (III) void fraction.

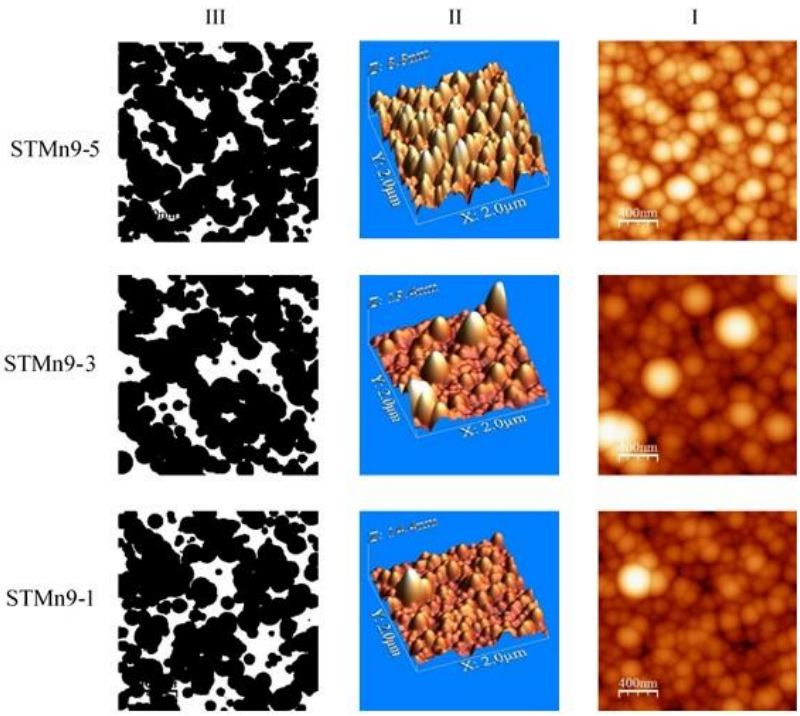

Fig. 6. AFM images of square tower-like Mn nanostructures produced at different distances of 1, 3 and 5 cm from the edge of the shadowing block with 9 arms; column (I) 2D images, column (II) 3D images, column (III) void fraction.

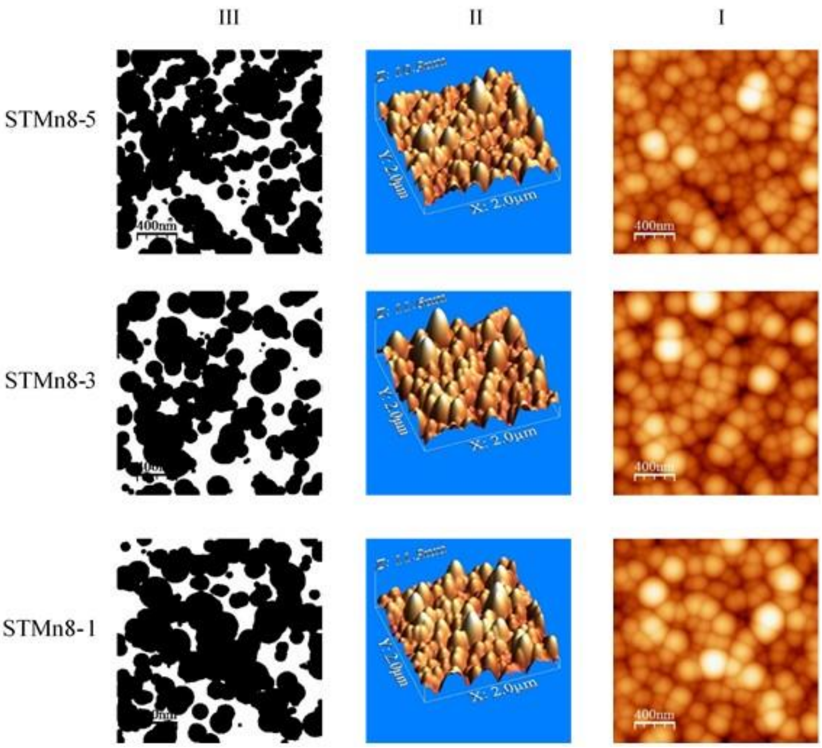

Fig. 7. AFM images of square tower-like Mn nanostructures produced at different distances of 1, 3 and 5 cm from the edge of the shadowing block with 8 arms; column (I) 2D images, column (II) 3D images, column (III) void fraction.

X-ray diffraction analysis

In Fig. 8 the x-ray diffraction patterns of the square tower-like manganese thin films with eight, nine and ten arms produced at three different distances of 1, 3 and 5 cm from the edge of the shadowing block. It can be observed that there is not much difference between samples at three different distances of 1, 3 and 5 cm from the edge of the shadowing block. The experimentally obtained values of crystallite size, lattice parameters and lattice strain from the x-ray diffraction peak of the samples are listed in Table 2. The highest intensity is obtained for the Mn (221), Mn (330), Mn (330) diffraction lines for the samples of STMn10, STMn9 and STMn8, respectively. The intensity of the main peak of STMn8 and STMn10 increases and STMn9 decreases with increasing the edge of the shadowing block. This indicates that the crystallinity degree of the STMn8 and STMn10 thin films increases while the STMn9 sample decreases with decreasing slope. Chaffar Akkari and et al. [5] reported that the degree of crystallinity of the Cu_2O zigzag thin films decreases at larger inclination angles, which is consistent with the results of the STMn8 and STMn10 samples in this work. The effect of the inclination angle (g) of the nanostructure for the production of architectural nanorods in this study shows that the maximum intensity of the main peak (330) in STMn8 nanostructures is higher and the intensity of this peak decreases with increasing number of arms from 8 arms to 9 arms and then the preferential orientation changes to (221) with increasing number of arms from 9 arms to 10 arms. This shows that the film is grown with a preferred orientation, though in case of sculptured thin films in which the axis of crystallography is inclined (changed) the proper identification of preferred orientation should be obtained by performing texture measurements.

The average diameter of crystallites (coherently diffracting domains), D_{xrd} may be calculated by using this diffraction line and the Sherrer equation [22]:

$$D_{xrd} = \frac{\kappa\lambda}{\beta\cos\theta} \tag{1}$$

where θ is the Bragg angle, κ is a dimensionless

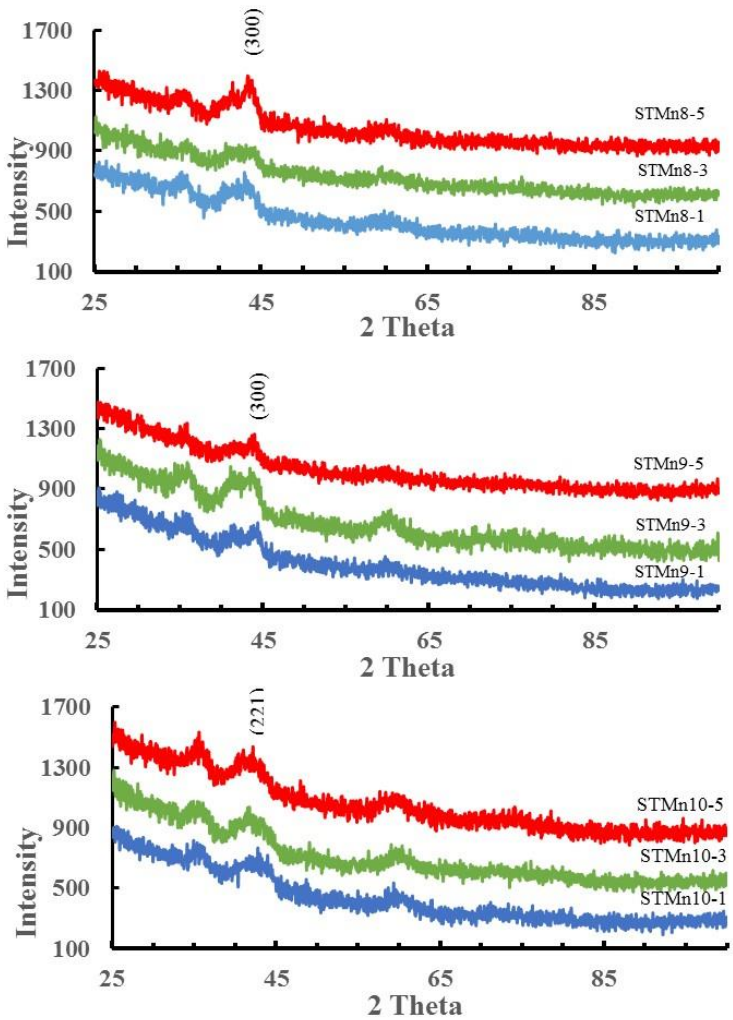

Fig. 8. XRD diffraction patterns of the square tower-like Mn nanostructures produced at different distances from the edge of the shadowing block with a) 8 arms, b) 9 arms and c) ten arms.

constant, which depends on the shape and crystal distribution and usually considered as unity, λ is the wavelength of the incident x-ray, and β is defined as;

$$\beta = \left(\omega_s^2 - \omega_0^2\right)^{1/2} \tag{2}$$

Where ω_0 and ω_s are the full width at half maximum (FWHM) of the diffraction line/peak of the stress-free standard sample and the sample produced in this work, respectively. Where ω_0 and ω_s are the full width at half maximum (FWHM) of the diffraction line/peak of the stress-free standard sample and the sample produced in this work, respectively.

In order to eliminate the broadening effect from the XRD device and structure defects [23, 24] the crystallite size was obtained using Williamson–Hall method. The total broadening b_{tot} is obtained by the following equation:

$$\beta_{tot}^2 = \beta_{crystallite}^2 + \beta_{stain}^2 + \beta_{instr}^2 \tag{3}$$

$$(\beta_{tot}^2 - \beta_{instr}^2)\cos^2\theta = (\frac{0.9\lambda}{D_{WH}})^2 + (4\varepsilon\sin\theta)^2 \tag{4}$$

Table 2. Experimentally obtained grain size and lattice strain of the square tower-like manganese thin films calculated from XRD data analysis

Assinged sample Code	Grain size			(h k l)	2θ (°)	d spacing	JCPDS card	Lattice strain (10^{-3})	Lattice strain-W_H (10^{-3})
	D_{AFM} (nm)	D_{Scher} (nm)	D_{W-H} (nm)						
Mn10-1	122.0	10.10	40.52	(2 2 1)	43.80	2.06382	00-033-0887	32.96	58.8
Mn10-3	112.0	9.32	20.26	(2 2 1)	41.50	2.17335	00-033-0887	27.98	57.1
Mn10-5	96.0	6.05	11.75	(2 2 1)	41.73	2.16289	00-033-0887	19.81	52
Mn9-1	120.7	6.23	19.16	(3 3 0)	43.89	2.06116	00-032-0637	16.93	36
Mn9-3	109.6	5.85	7.54	(3 3 0)	43.62	2.07336	00-032-0637	18.96	42.1
Mn9-5	81.0	5.52	7.42	(3 3 0)	43.80	2.06543	00-032-0637	19.09	46.1
Mn8-1	132.3	11.08	35	(3 3 0)	43.40	2.08541	00-032-0637	13.47	27.1
Mn8-3	128.9	10.43	11.07	(3 3 0)	43.90	2.05936	00-032-0637	13.15	19
Mn8-5	91.9	6.95	9.66	(3 3 0)	43.63	2.07269	00-032-0637	7.42	7.1

D_{AFM} is grain size obtained from AFM analysis.

$(\beta_{tot}^2 - \beta_{instr}^2)\cos^2\theta$ versus $\sin^2\theta$ is plotted and we get a linear curve. From the slope of the line, the amount of strain and from the intercept, the crystallite size is calculated. Due to considering the strain correction factor in Williamson–Hall method, the crystallite size obtained by the Scherrer's formula (coherently diffracting domain) is less than Williamson–Hall method. However, in both methods the crystallite size decreases with increasing distance from the edge of the shadowing block. Also, the grain size obtained from AFM images is reduced by increasing the distance from the edge of the shadowing block, which is consistent with the results of Scherrer and Williamson–Hall method (Table 2). It should be noted that in thin films of STMn each grain is composed of several crystalitte, so the grain size and crystalitte size are not the same.

When the number of arms increases from 8 to 9 arms, the grain size and the crystallite size decrease and as the number of arms increases from 9 to 10 arms, the grain size and the crystallite size increase for corresponding distances from the edge of the shadowing block.

The strain value obtained for all samples is given in Table 2. The results show that the strain on the nanostructures of the STMn8 and STMn10 decreases with increasing distance from the edge of the shadowing block (decreasing the slope of nanostructure) due to the increase in the intensity of the main peak. While strain on the nanostructure of the STMn9 increases with increasing distance from the edge of the shadowing block due to the decrease in the intensity of the main peak. Since the preferred growth orientation for nanostructures of the STMn8 and STMn9 is in the orientation (330), the strain is increased with increasing number of arms from 8 to 9 arms for corresponding distances from the edge of the shadowing block. While strain is increased by increasing the arm number from 9 to 10 arms. This may be due to a change in the preferred growth orientation in the nanostructure of the STMn10 to (221) diffraction orientation/plane.

CONCLUSION

The results of this study can be summarized as follows:

1. A GLAD deposition process with a shadowing block fixed at the centre of the substrate holder was successfully proposed to prepare square tower-like manganese thin films in the room temperature.
2. Three different square tower-like thin films containing different number of arms, namely eight, nine and ten arms with different slopes were produced.
3. Results showed that the slope angle (a), the grain size, porosity and surface roughness of the films decreases with decreasing the slope of nanostructure.
4. The effect of the inclination angle (g) of the nanostructure shows that the maximum intensity of the main peak (330) in STMn

nanostructures with 8 arms is higher and the intensity of this peak decreases with increasing number of arms from 8 arms to 9 arms and then the preferential orientation changes to (221) with increasing number of arms from 9 arms to 10 arms.

5. The strain on the nanostructures of the STMn with 8 and 10 arms decreases with increasing distance from the edge of the shadowing block due to the increase in the intensity of the main peak. While strain on the nanostructure of the STMn with 9 arms increases with decreasing the slope of nanostructure.

CONFLICT OF INTEREST STATEMENT

All authors declare that no conflicts of interest exist for the publication of this manuscript.

REFERENCES

[1] Robbie K, Brett MJ. Sculptured thin films and glancing angle deposition: Growth mechanics and applications. Journal of Vacuum Science & Technology A: Vacuum, Surfaces, and Films. 1997; 15(3): 1460-1465.

[2] Robbie K, Brett MJ, Lakhtakia A. Chiral sculptured thin films. Nature. 1996; 384(6610): 616-616.

[3] Ghosh A, Murkute P, Lahiri R, Chakrabarti S, Chattopadhyay KK, Mondal A. GLAD synthesised erbium doped In_2O_3 nano-columns for UV detection. Journal of Materials Science: Materials in Electronics. 2019; 30(13): 12739-12752.

[4] Sinaoui A, Chaffar-Akkari F, Gallas B, Demaille D, Kanzari M. Investigation of growth and characterization of nanostructured CuIn5S8 thin films produced by glancing angle deposition. Thin Solid Films. 2015; 590: 111-117.

[5] Akkari FC, Jbara HB, Abdelkader D, Gallas B, Kanzari M. Effect of angle deposition γ on the structural, optical and electrical properties of copper oxide zigzag (+ γ,− γ) nanostructures elaborated by glancing angle deposition. Thin Solid Films. 2018; 657: 61-69.

[6] Babaei F, Savaloni H. Optical absorption transitions in Mn star-like helical sculptured thin films. Plasmonics. 2018; 13(1): 203-214.

[7] Chen CW, Tsai HW, Wang YC, Su TY, Yang CH, Lin WS, Chueh YL. Design of novel TiO_2–SiO_2 core–shell helical nanostructured anti-reflective coatings on Cu (In, Ga) Se_2 solar cells with enhanced power conversion efficiency. Journal of materials chemistry A. 2019

[8] Muhammad Z, Ali MW, Ullah K, Kumar S, Zhu L. Narrowing of filters and laser mirror in tilt-modulated chiral sculptured thin films. Optics Communications. 2020; 125927.

[9] Savaloni H, Savari R, Abbasi S. Application of Mn nano-flower sculptured thin films produced on interdigitated pattern as cathode and anode electrodes in field ionization gas sensor. Current Applied Physics. 2018; 18(8): 869-878.

[10] Hu Y, Wu Y, Wang J. Manganese-Oxide-Based Electrode Materials for Energy Storage Applications: How Close Are We to the Theoretical Capacitance?. Advanced Materials. 2018; 30(47): 1802569.

[11] Mane VJ, Malavekar DB, Ubale SB, LokhandeVC, Lokhande CD. Manganese dioxide thin films deposited by chemical bath and successive ionic layer adsorption and reaction deposition methods and their supercapacitive performance. Inorganic Chemistry Communications. 2020; 115: 107853.

[12] Bhat SS, Masih P, Shah MA. Study of magnetic properties of iron doped of manganese oxide nanoparticles: Growth and characterization. 2019

[13] Yin Y, Wu J, Zhou W, Ma W, Jiang L, Gao Y, Huang Z. Effects of deposition temperature on microstructure, cation distribution and electrical properties of Mn1. 56Co0. 96Ni0. 48O4 thin films grown by RF magnetron sputtering. Journal of Alloys and Compounds. 2020; 153705.

[14] Di W, Liu F, Lin T, Kong H, Meng C, Zhang W, Hou Y. Influence of oxygen partial pressure on structural and electrical properties of Mn1. 56Co0. 96Ni0. 48O4 thin films deposited by pulsed laser deposition. Applied Surface Science. 2018; 447: 287-291.

[15] Li YW, Qiao Q, Zhang JZ, Hu ZG, Chu JH. Influence of post-annealing on structural, electrical and optical properties of manganese oxide thin films grown by atomic layer deposition. Thin Solid Films. 2015; 574; 115-119.

[16] Alié C, Calberg C, Páez C, Liquet D, Eskenazi D, Heinrichs B, Job N. Electrochemical performances of Li4Mn5O12 films prepared by spray-coated sol-gel reaction. Journal of Power Sources. 2018; 403: 173-183.

[17] Krause KM, Brett MJ. Spatially graded nanostructured chiral films as tunable circular polarizers. Advanced Functional Materials. 2008; 18(20): 3111-3118.

[18] Savaloni H, Esfandiar A. Fabrication, characterization and some applications of graded chiral zigzag shaped nano-sculptured silver thin films. Applied surface science. 2011; 257(22): 9425-9434.

[19] Savaloni H, Babaei F, Song S, Placido F. Characteristics of sculptured Cu thin films and their optical properties as a function of deposition rate. Applied Surface Science. 2009; 255(18): 8041-8047.

[20] Alouach H, Mankey GJ. Texture orientation of glancing angle deposited copper nanowire arrays. Journal of Vacuum Science & Technology A: Vacuum, Surfaces, and Films. 2004; 22(4): 1379-1382.

[21] Esfandiar A, Savaloni H, Placido F. On the fabrication and characterization of graded slanted chiral nano-sculptured silver thin films. Physica E: Low-dimensional Systems and Nanostructures. 2013; 50: 88-96.

[22] Ingham B. X-ray scattering characterisation of nanoparticles. Crystallography Reviews. 2015; 21(4): 229-303.

[23] Karen P, Woodward PM. Liquid-mix disorder in crystalline solids: ScMnO3. Journal of Solid State Chemistry. 1998; 141(1): 78-88.

[24] Theivasanthi T, Alagar M. Electrolytic synthesis and characterizations of silver nanopowder. Nano Biomed. Eng. 2012; 4: 58–65.